Icarus 252 (2015) 175–185

Contents lists available at ScienceDirect

Icarus

journal homepage: www.elsevier.com/locate/icarus

# Evidence for an explosive origin of central pit craters on Mars

Nathan R. Williams *, James F. Bell III, Philip R. Christensen, Jack D. Farmer

*School of Earth and Space Exploration, Arizona State University, Tempe, AZ 85287, USA*

ARTICLE INFO

*Article history:*
Received 15 April 2014
Revised 27 November 2014
Accepted 2 December 2014
Available online 9 December 2014

*Keyword:*
Mars
Impact processes
Cratering

ABSTRACT

Kilometer-scale pits are nested in the centers of many impact craters on Mars as well as on icy satellites. They have been inferred to form in the presence of a water–ice rich substrate; however, the process(es) responsible for their formation is still debated. Previous models invoke origins by either explosive excavation of potentially water-bearing crustal material, or by subsurface drainage of meltwater and/or collapse. If explosive excavation forms central pits, pit-derived ejecta should be draped around the pits, whereas internal collapse should not deposit significant material outside pit rims. Using visible wavelength images from the Mars Reconnaissance Orbiter (MRO) Context Camera (CTX) and High Resolution Imaging Science Experiment (HiRISE) instruments and thermal infrared images from the Odyssey Thermal Emission Imaging System (THEMIS) instrument, we conducted a survey to characterize, in detail, the global population of central pits in impact craters $\geqslant$10 km in diameter. We specifically examined the morphology and thermophysical characteristics of the pits for evidence of pit ejecta. Our analysis of thermal images suggests that coarse-grained materials are distributed proximally around many central pits on the floors of their host craters. The decrease in average grain size with distance from pit rims is consistent with pit-derived ejecta. These observations and interpretations better support an explosive origin for central pits on Mars than they do an origin of subsurface meltwater drainage and collapse of the overlying substrate. A major weakness to previous explosive central pit formation models is the inability for them to form pits late enough in the impact process to be preserved. To address this, we present an alternative "melt contact model" where a central uplift brings ice-bearing substrate into contact with impact melt to generate steam explosions and excavate central pits during the impact modification stage. Theoretical calculations show that more than enough thermal energy is available via impact melt from the host crater to form central pits by steam explosions, and such explosions would require only a modest amount (2–6% by volume) of uplifted water–ice. We therefore propose that central pits on Mars could have formed explosively by the interaction of impact melt and subsurface water–ice.



## 1. Introduction

Kilometer-scale pits are centered in many impact craters on Mars and have remained enigmatic structures for several decades. Their formation is often hypothesized to be connected with subsurface water due to their relative abundance on Mars and icy satellites and scarcity on other rocky bodies, but the role of water and the specific process(es) responsible for forming central pits are still debated. In this study, we make thermal inertia observations of central pit craters to test hypotheses for central pit formation. We start with an overview of the previously proposed hypotheses and the gaps in our understanding. Then, we discuss the utility of thermal inertia in remotely determining grain size distributions around central pits to test formation models.

## 2. Background

Central pits occur in many impact structures on Mars and exhibit a crater-in-crater configuration (*e.g.*: Smith, 1976; Hodges, 1978; Barlow, 2006, 2010) (Fig. 1). Kilometer-scale central pits have been identified on the floors or on tops of the central peaks of over 1000 martian impact craters with diameters as large as 125 km in diameter and down to as small as 5 km in diameter (Smith, 1976; Barlow and Bradley, 1990; Barlow et al., 2000; Barlow, 2011), although some smaller central pits have also been identified (Barlow, 2010). In our study, we focus on "floor pits" that are deeper than the surrounding floors of their host craters, as opposed to "summit pits" that occur atop central peaks and have floors at higher elevations than their host crater floors, to avoid potential bias in our thermal methods due to coherent rock or boulders on the sides of the central peaks. Based an ongoing survey by Barlow (2010, 2011) and this study, central floor pits have a

* Corresponding author.

http://dx.doi.org/10.1016/j.icarus.2014.12.005
0019-1035/

median diameter of 0.16–0.175 host crater radii, such that a 50 km diameter crater might have a central pit ~8 km wide. Their depths range from very shallow to over 1.5 km below the surrounding impact crater floor, measured using Mars Orbiter Laser Altimeter data (Smith et al., 2001) for a few of the largest central pits [this study].

Central pit craters on Mars are confined to low and mid-latitudes, within ±70° of the martian equator (Hodges et al., 1980; Barlow, 2011; Garner and Barlow, 2012). They are also common for impact craters on icy satellites, including Ganymede and Callisto (Smith et al., 1979). Central pits are seldom observed on rocky planets other than Mars, although a few dozen are present on Mercury (Schultz, 1988; Xiao and Komatsu, 2013) and the Moon (Croft, 1981; Schultz, 1976a,b, 1988; Xiao et al., 2014). As a result, several proposed models require water to play a leading role in forming central pits.

The presence of water–ice has been believed to be involved in typical pit formation for decades (Hodges et al., 1980; Croft, 1981). Although water–ice is not stable at the surface of Mars within the low latitudes today (Clifford and Hillel, 1983; Mellon et al., 1997; Head et al., 2003), water was (and may still be) present within the upper few meters to kilometers of the surface even at low latitudes earlier in Mars' history. The possibility of significant subsurface water in pre-impact terrains is supported by the presence of layered ejecta surrounding many fresh martian impact craters (Carr et al., 1977; Gault and Greeley, 1978; Wohletz and Sheridan, 1983; Barlow et al., 2000; Baloga et al., 2005) and Mars Odyssey Gamma Ray Spectrometer spectra (Boynton et al., 2007). However, the process(es) responsible for forming central pits in impact craters and the role of water are still debated, and several mechanisms for pit formation have previously been proposed.

Wood et al. (1978) proposed that explosive decompression may volatilize a subsurface water-rich layer, causing steam explosions and removing the core of central peaks. However, this explosive model suffers from the difficulty of keeping water vapor from escaping early in the impact process before a central pit can be preserved (Croft, 1981; Pierazzo et al., 2005; Senft and Stewart, 2011; Elder et al., 2012).

Croft (1981), Bray (2009), Senft and Stewart (2011), Alzate and Barlow (2011) and Elder et al. (2012) proposed that central pits could form by the melting then gravitational drainage of target water–ice through fractures underlying central uplifts. This model provides a low-energy solution to forming central pits long enough after impact that they should be preserved. However, raised rims are also associated with many martian central pits (Wood et al., 1978; Garner and Barlow, 2012) and would not be expected with drainage structures. These models also require large volumes of water to be drained, nearly equal to the volumes of the central pits plus any initial central peaks, which is unrealistic for forming the central pits on the Moon and Mercury assuming pits there form by the same mechanism as on Mars. Numerical simulations of the melt-drainage model have also only been successful in predicting central pits when conducted for pure-ice targets.

Passey and Shoemaker (1982), Greeley et al. (1982), and Bray et al. (2012) proposed that central peaks of impacts in weak target materials may collapse to form central pits. This model explains the destruction of central peaks in craters that might otherwise have them. However, the abundance of impact craters with central peaks and summit pits in the same regions as impact craters with floor pits suggests that the target material should be strong enough to prevent collapse (Barlow, 2011).

Greeley et al. (1982) proposed and demonstrated in laboratory experiments that small-scale central pits can be excavated from impacts into layered targets, causing central peaks to detach, rise directly upwards, and fall back into the crater bowl forming a central secondary pit. This model does not require a target to be water-bearing, consistent with the presence of a small number of central pits on Mercury and the Moon, although a water-bearing layer could provide an enhancing strength contrast. However, scaling up to planetary impact craters with diameters of tens of kilometers is problematic because of the scale-dependent magnitude of gravitational versus strength-limited late-stage impact modification, greatly reducing the influence of any layer strength differences on the final crater morphology (Croft, 1981).

Schultz (1988) proposed that central pits are excavated as a primary result of impacts with low-velocity bolides. This model also does not require a target to be water-bearing, and implies that the presence yet relative scarcity of central pits on Mercury and the Moon compared to icy satellites is due to higher average impact velocities in the inner Solar System. However, Schultz (1988) assumes that post-impact modification is only weakly dependent on crater size, which becomes an issue for craters with diameters of tens of kilometers (Croft, 1981).

Each of the above models has both strengths and weaknesses. We provide another set of observations to test these models using new thermal observations and test for the presence or absence of ejecta. For this study, we broadly group the previously proposed mechanisms for pit formation into those that explosively eject pit material up and outward (*e.g.*: Wood et al., 1978; Greeley et al., 1982; Schultz, 1988) versus those that drain or collapse material downward (*e.g.*: Croft, 1981; Passey and Shoemaker, 1982). During a crater-forming explosion, rocks and boulders are ejected out of the crater, layers are proximally uplifted and overturned, and ejecta are draped over the surrounding surface (*e.g.* Melosh, 1989). Raised rims can be formed by both the addition of ejecta (*e.g.* White and Ross, 2011) and structural uplift (Sharpton, 2014), although the latter indicates that the uplift is the greatest contributor to raised impact rims for impacts. The average grain size for ejecta decreases with radial distance from the crater, such that the largest clasts or blocks are proximal to the crater rim (*e.g.*: Gault et al., 1963; O'Keefe and Ahrens, 1985; Melosh, 1989; Buhl et al., 2014). Conversely, drainage and collapse

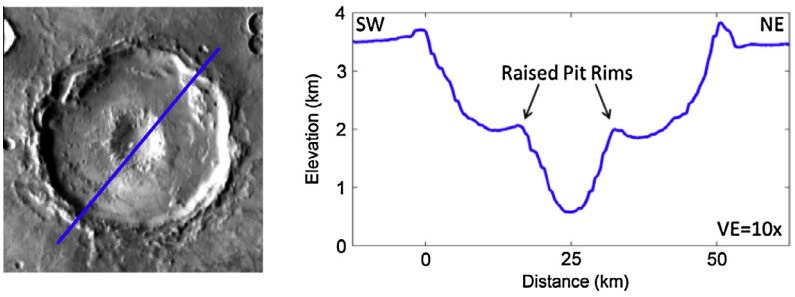


**Fig. 1.** THEMIS daytime IR mosaic of a 50 km diameter unnamed martian impact crater containing a central pit at 296.4°E, 17.6°S. A MOLA topographic profile across the center shows typical pit morphology.

features such as sinkholes, which are typical of karst landscapes, and lava tube skylights form by gravitational collapse and do not create raised rims nor emplace material atop their rims (*e.g.*, Okubo and Martel, 1998; Salvati and Sasowsky, 2002; Cushing et al., 2007; Robinson et al., 2012). The presence or absence of pit-derived ejecta around central pits therefore provides one way to distinguish between explosive versus drainage and collapse scenarios for the formation of central pits.

We use the presence or absence of decreasing average grain size with distance from pits as the indicator of possible pit-derived ejecta. We hypothesize that central pits are formed by explosive excavation or devolatilization during or after impact. The Wood et al. (1978), Greeley et al. (1982) and Schultz (1988) models would be supported by the presence of pit-derived ejecta, and the Croft (1981) and Passey and Shoemaker (1982) models would not be supported. After analyzing our results, we also address the weakness of previous explosive formation models to produce central pits late enough in the impact process to be preserved, by presenting an alternative "melt contact model" for central pit formation late in the impact process. Finally, we apply our integrated observations to interpret the morphology and thermal properties of central pits in the context of central uplifts and propose testable predictions for the model.

## 3. Data and methods

For this study, we surveyed impact craters >~10 km in diameter and identified central floor pits within ±60° latitude of the martian equator using the Java-based planetary geographic information system program JMARS (Christensen et al., 2009). Central pits were identified as distinctive circular depressions in the center of an impact crater that appeared to be deeper than the host crater floor based on the available imaging and topography. Many small impact craters with diameters <10 km containing central depressions were excluded from our survey due to poor spatial resolution, as well as craters we could not confidently determine had depressions deeper than the host floor. We excluded summit pits that occur atop central peaks and are not deeper than the host crater floor to avoid potential bias from coherent rock or boulders exposed on or eroding out of the sides of the central peaks. We also excluded structures that we considered to be peak rings for large host craters with diameter of several tens of kilometers, and concentric terraces, especially in craters near the martian simple to complex crater transition of ~6–7 km diameter (Garvin et al., 2000a,b).

Diameters were measured for both the central pits and their host craters. Only the largest central pits are resolved in the 128 pixel/deg (460 m/px) Mars Orbiter Laser Altimeter (MOLA) global mosaic (Smith et al., 2001), so the ~100 m/pixel Mars Odyssey mission Thermal Emission Imaging Spectrometer (THEMIS) (Christensen et al., 2004) calibrated daytime infrared (IR) global mosaic (Edwards et al., 2011) was used for most craters, which provides nearly complete (~90%) coverage to ±60° latitude. THEMIS daytime IR images show topography as shading, since Sun-facing slopes are warmer and have the highest pixel values, while slopes facing away from the Sun or those in shade are coolest and have the lowest pixel values. Higher resolution visible images were also used to observe finer-scale morphology and distinguish central morphologies that appeared ambiguous in THEMIS daytime IR. Primarily, we used Mars Reconnaissance Orbiter mission Context Camera (CTX) (Malin et al., 2007; Bell et al., 2013) images at ~6 m/pixel that were map-projected and photometrically stretched from Planetary Data System (PDS) raw electronic data records, and where available we used High Resolution Imaging Science Experiment (HiRISE) (McEwen et al., 2007) images at ~0.25–1.3 m/pixel that were map-projected and photometrically stretched from PDS calibrated reduced data records. The global dust environment for central pit crater context is shown using Thermal Emission Spectrometer (TES) solar energy reflectivity (albedo) integrated from 0.3 to 2.9 μm (Christensen et al., 2001).

During the formation of impact and other explosive craters, coarse debris are typically ejected and scattered outside the crater. Large blocks and coarse grains have a higher thermal inertia than finer-grained materials and hold on to their heat longer through the night. Thermal conductivity, a function of grain size, varies by 3–4 orders of magnitude more than density and specific heat for geologic materials under martian atmospheric conditions. As a result, thermal inertia calculated from nighttime thermal images can be used to estimate changes in average grain size (Christensen, 1986). We therefore used the THEMIS thermal inertia global mosaic as a quantitative proxy for average grain size, such that coarse-grained or blocky materials have relatively higher thermal inertias (warmer at night) while dust, sand, and other fine-grained materials have lower thermal inertias (cooler at night) (Christensen, 1986; Fergason et al., 2006; Edwards et al., 2009, 2011). THEMIS nighttime images and thermal inertias have previously been used to identify blocky ejecta rays from impact craters on Mars that otherwise show little or no albedo variation in visible images but where grain size trends are seen with respect to distance from the crater (McEwen et al., 2005; Tornabene et al., 2006). Central pits with an annulus or a geographically skewed patch of higher thermal inertia material nearer the pit rim than more distally across the surrounding host crater floor may be classified as having a fining average grain size with radial distance, consistent with ejecta.

To measure the trend of thermal inertias, we circumferentially averaged the THEMIS thermal inertia mosaic over central pit craters in intervals of 0.1 host crater radii. Because most central pits are <0.2 crater radii, we compared pit-proximal averaged thermal inertia values within the interval from 0.2 to 0.3 crater radii versus more distal averaged thermal inertia values at 0.5–0.6 crater radii. A Student's *t*-test was then performed on the differences between proximal and distal averaged thermal inertias for the population of central pits. A significance level of $P \geqslant 0.05$ would be deemed not statistically significant and served as our null hypothesis: thermal inertia and average grain size do not decrease radially away from pit rims. For $P < 0.05$, a radial decrease in thermal inertia with distance from the pit rim would be deemed statistically significant and we would reject the null hypothesis and support an alternative hypothesis that ejecta surrounds central pits.

## 4. Results

We identified central floor pits within 654 host craters ~10 km diameter or larger between ±60° latitude of the martian equator (Fig. 2). Additional smaller craters with central pits exist (Barlow, 2010, 2011), but are not well-resolved in the THEMIS thermal images used for this study. MOLA topographic profiles have very coarse resolution and may only provide topographic insight to the largest central pit craters (Fig. 1), and sometimes show complete and partially rimmed pits that frequently occur in the highlands terrains (Garner and Barlow, 2012). We identified central pits in host impact craters with diameters ranging from ~8 to 114 km, with 95% of those host craters being <50 km in diameter and excluding smaller potential central pit craters. The surveyed central pits have a median diameter ratio to their host craters of 0.175 with a standard deviation of 0.037 (Fig. 3). These results are comparable to the median ratio of 0.16 found by Barlow (2011).

Based on THEMIS-derived thermal inertias, most central pits showed higher thermal inertia (coarser) material near their rim

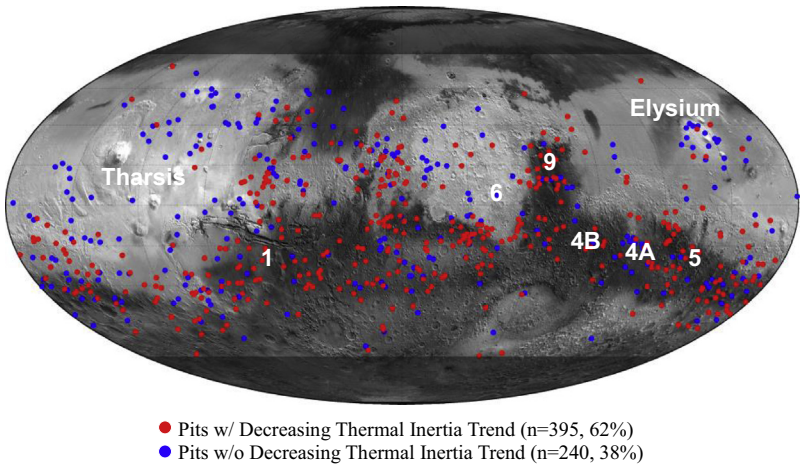


**Fig. 2.** Distribution of 654 central pit craters identified in our survey of the THEMIS daytime global mosaic, within ±60° of the martian equator, overlain on the TES albedo basemap (Christensen et al., 2001) and presented in a Mollweide equal area projection. Locations of Figs. 1, 4A, B, 5, 6, and 9 are highlighted. The Tharsis and Elysium regions are also labeled, where coatings of dust mask most central pit thermal signatures.

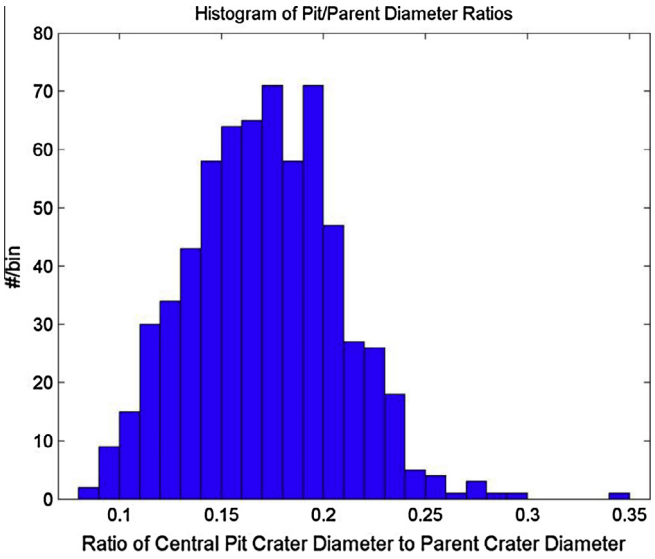


**Fig. 3.** Histogram showing the range of diameter ratios between central pits and their host craters that we measured. The median value is 0.175 with a standard deviation of 0.037.

than more distally on the host crater floor (*e.g.* Fig. 4). 635 of the 654 central pits had thermal images over their host crater floors. A number of observations can be seen in our data. A majority of CPCs (62%, $n$ = 395) show radially decreasing thermal inertia trends outside the pits. That percentage increases to 76% (254 of 333) with increasing host crater diameter (>20 km). Restricting the selection of central pits craters to those with absolute thermal inertia values >300 TIU (coarser than medium-grained sand and dust), independent of crater diameter, increases the percentage to 80% (175 of 216). Central pit craters with both host crater diameters >20 km and absolute thermal inertia values >300 TIU increases the percentage to 89% (74 of 83). Pits with proximal high and radially decreasing thermal inertias in THEMIS images show large blocky debris (up to tens of meters wide) in visible CTX and HiRISE images (Fig. 5), while pits that did not show proximally high nor decreasing thermal inertias appear blanketed or mantled (Fig. 6).

We conducted a paired Student's $t$-test to determine the confidence interval of the measured thermal inertia decreases from 0.2–0.3 crater radii to 0.5–0.6 crater radii. For the 635 central pit craters with thermal images, the $t$-test returns a $P < 0.01$ indicating extreme statistical significance. We therefore reject our null hypothesis that thermal inertia and average grain size do not decrease radially away from pit rims, and adopt an alternative hypothesis that pits are surrounded by ejecta with grain size decreasing with distance away from the pit.

The median proximal thermal inertia for central pits with radially decreasing thermal inertias is 283 thermal inertia units (1 TIU = 1 J m$^{-2}$ K$^{-1}$ s$^{-1/2}$) with a standard deviation of 121 TIU, while the median proximal thermal inertia for central pits with other, radially non-decreasing thermal inertia trends is 205 TIU with a standard deviation of 145 TIU (Fig. 7). Central pits lacking the radially decreasing trends are more common in Tharsis, Elysium, and other dusty regions characterized by high TES albedos and low thermal inertia values (blue[1] dots around "Tharsis" and "Elysium" in Fig. 2).

Smaller central pits also tend not to show radially decreasing thermal inertias (Fig. 8). Based on the population of impact craters observed with THEMIS data, the median diameter for host craters containing pits with warm material is ~23.3 km and the median diameter for craters with pits lacking it is ~16.7 km, both cases being above the simple/complex transition of 6–7 km for martian craters (Garvin et al., 2000a,b).

## 5. Discussion

The raised rims around some pits (Wood et al., 1978; Garner and Barlow, 2012) are suggestive of explosive excavation, similar to their host craters, which also have raised rims. As discussed by Garner and Barlow (2012), raised rims are more frequently observed in larger central pits than smaller ones. They also argue that the preferred distribution of rimmed pits in highlands regions and non-rimmed pits in volcanic plains suggests that target material strength and/or volatile content may also limit the expression of raised rims. Some very small scale pits on Mars believed to have formed from volatile release in impact melt have been identified and also exhibit slightly raised rims, although they are not exclusive to crater centers and do not exhibit well-defined ejecta (Tornabene et al., 2012; Boyce et al., 2012). Surfaces visible in some CTX and HiRISE images show large (meter-scale) blocks in warm

[1] For interpretation of color in Fig. 2, the reader is referred to the web version of this article.

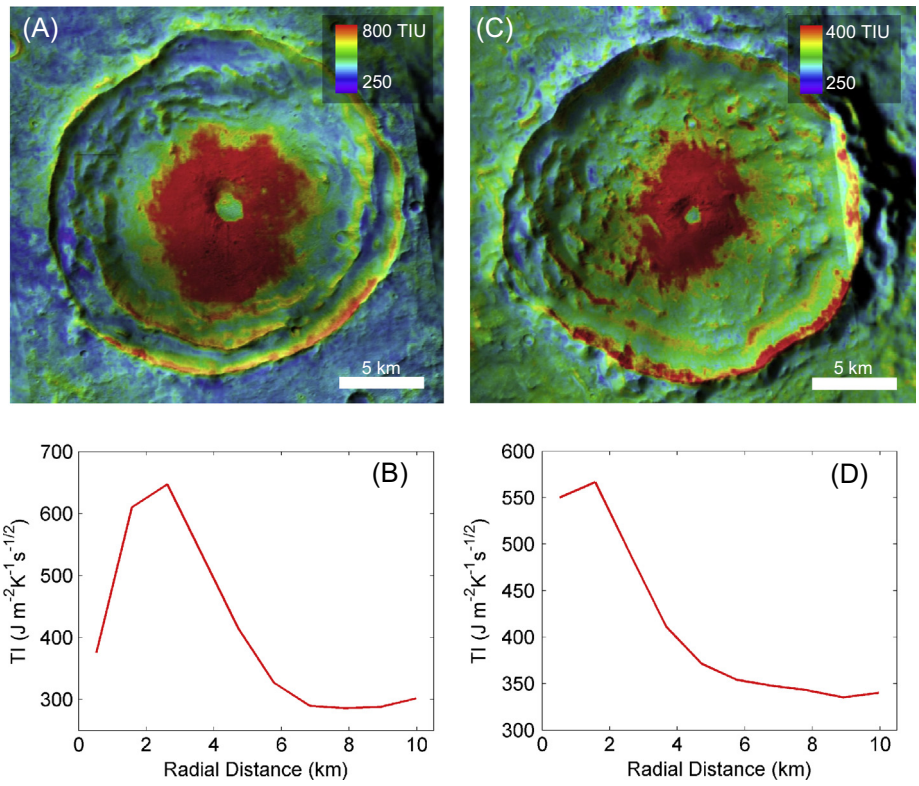


**Fig. 4.** THEMIS nighttime (color) and CTX visible (shading) images showing radially decreasing high thermal inertia material interpreted as ejecta surrounding two central pit craters at (A) 18.4°S, 102.7°E, and (C) 14.9°S, 93.2°E. Color scales indicate thermal inertia values. Panels (B) and (D) show the radially decreasing thermal inertia trends for the central pit craters in (A) and (C), resp. (For interpretation of the references to color in this figure legend, the reader is referred to the web version of this article.)

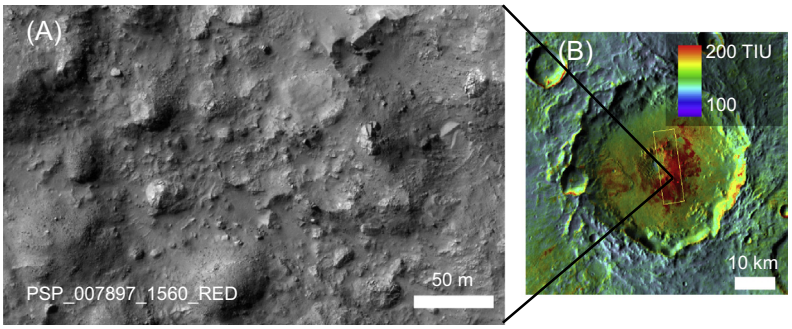


**Fig. 5.** (A) HiRISE image showing large blocks near a central pit crater at 23.8°S, 126.8°E. (B) THEMIS nighttime IR (color) over daytime IR (shading) context image showing high-thermal inertia material inferred as being blocky and confirmed by the HiRISE image. Black lines indicate location of A. Yellow box in B indicates footprint of HiRISE image. (For interpretation of the references to color in this figure legend, the reader is referred to the web version of this article.)

patches adjacent to central pits (*e.g.*, Fig. 5), consistent with the expected correlation between warm material and coarse surfaces. Such blocks and megablocks are commonly observed near impact craters, including at the Ries crater in Germany (*e.g.* Gault et al., 1963) and at some martian craters (*e.g.*, Caudill et al., 2012). Combined with the spatial correlation of warm material and central pits, we interpret the blocks scattered around central pits to be explosively-emplaced pit ejecta.

The observability of high thermal inertia, coarse-grained material appears linked to the size of the pit. Small craters excavate smaller volumes of material that is finer-grained on average than larger craters (*e.g.*: Gault et al., 1963; O'Keefe and Ahrens, 1985; Melosh, 1989; Buhl et al., 2014). Fine-grained rocks are more easily eroded or buried than coarser-grained rocks, so the coarser ejecta at larger pits should be preferentially preserved and less buried. Surface diurnal thermal inertias are sensitive to materials within a few thermal skin depths (several centimeters) of the surface, so any ejecta would have to be buried by no more than a few centimeters of dust in order to be observable. Accumulated dust and sand is frequently observed on Mars and is indicated in our analysis as low thermal inertia values due to dust's fine grain size (Fig. 6). The smaller grain size distribution of ejecta for smaller craters is therefore expected to decrease the positive detection of ejecta using diurnal thermal inertias.

The presence of high thermal inertia material on host crater floors near pits would not necessarily need to be due to pit-derived ejecta. To avoid many false-positives, we have calculated the trend in thermal inertia (grain size) with radial distance from the pit. For example, post-impact lava or perhaps impact melt flows occur on the floors of some craters containing central and have high thermal inertias, although small flow lobes are easily distinguishable (Fig. 9), and much more extensive lava or impact melt flows could

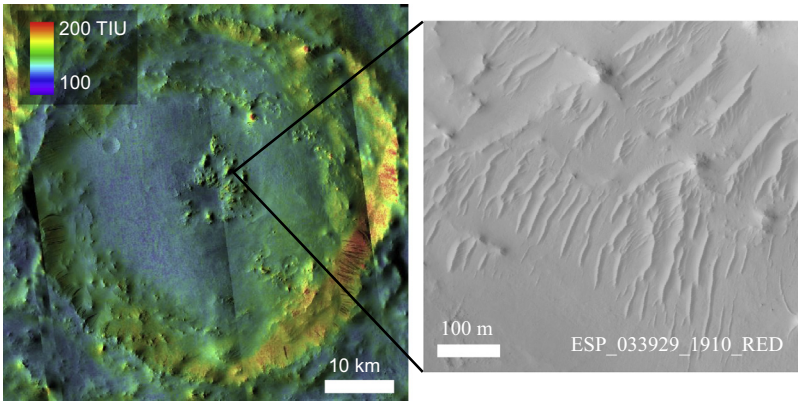


**Fig. 6.** (A) THEMIS nighttime IR (color) over CTX visible (shading) image showing a central pit crater at 10.9°N, 50.8°E without a radially decreasing thermal inertia. Average thermal inertia values are uniformly low across the crater floor and associated with a coating of fine-grained dust. (B) HiRISE visible image enlargement of an area near the central pit showing low-contrast dust mantling the terrain. (For interpretation of the references to color in this figure legend, the reader is referred to the web version of this article.)

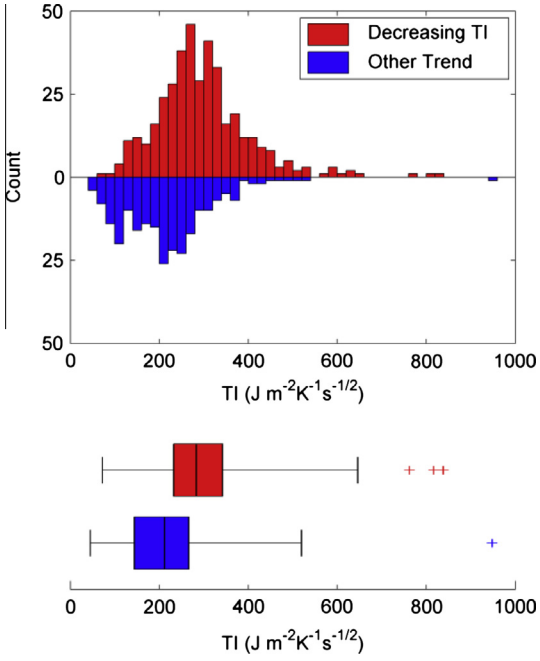


**Fig. 7.** Histogram and box-and-whisker plot of central pit craters exhibiting radially decreasing thermal inertia trends (red) and radially non-decreasing thermal inertia trends (blue) plotted against THEMIS thermal inertia values. Lower thermal inertias are indicative of finer average grain size and dustiness. (For interpretation of the references to color in this figure legend, the reader is referred to the web version of this article.)

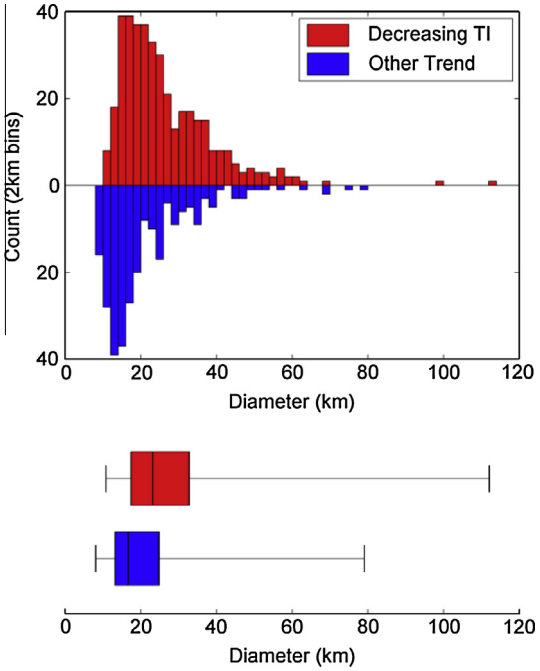


**Fig. 8.** Histogram and box-and-whisker plot of craters containing central pits exhibiting radially decreasing thermal inertia trends (red) and radially non-decreasing thermal inertia trends (blue) plotted against host crater diameter. (For interpretation of the references to color in this figure legend, the reader is referred to the web version of this article.)

potentially fill central pits. We expect impact melt ponds to be distributed throughout the crater floor, so measuring a radially decreasing trend in thermal inertia as opposed to only using high thermal inertia values avoids this problem in most cases.

Mass wasting of material off the host crater wall is also unlikely to cause a radially decreasing thermal inertia trend, as the coarsest materials slumping off the wall should be distributed closer to the source walls and far from central pits, instead making a radially increasing trend. Similarly, we expect that blocky material transported fluvially or glacially from outside the crater and down the crater walls should be preferentially deposited with the coarsest grains near the break in slope at the base of the crater wall, far from central pits. If a central peak did form and shed material before the peak's destruction, that material might be manifested on the floor of the host crater at the base of the now-destroyed central peak. However, we expect any gravitational or fluid-driven transport of such peak material would be very limited before collapse of any central peaks to possibly form pits. Patchy or partial erosional uncovering of consolidated host crater fill rocks could also explain higher thermal inertias relative to the surrounding crater floor; however, we consider the selective removal of significant amounts of dust from the centers of host craters, but not in the dusty plains surrounding many host craters, to be unlikely. Additionally, significant erosion on the host crater floor is inconsistent with the presence and preservation of raised rims around many central pits. Thermal inertias are also low for relatively fine-grained aeolian dunes or other bedforms that often form in the centers of craters, and confirmed in CTX and HiRISE images (Fig. 6).

For central pit craters on Mars, the radial decrease of thermal inertia is consistent with and supports the Wood et al. (1978),

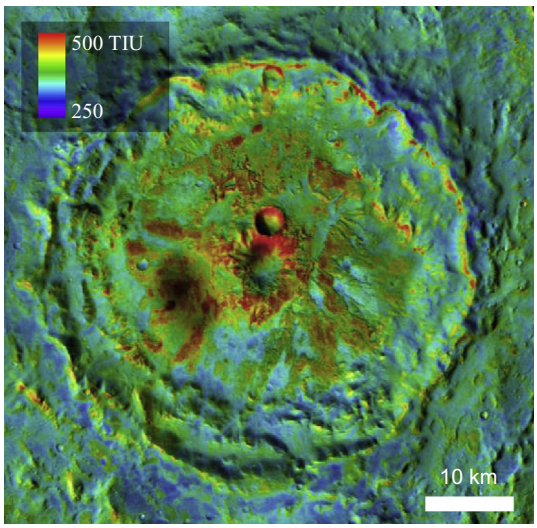


**Fig. 9.** THEMIS nighttime IR (color) over CTX visible (shading) image showing high thermal inertia lava or impact melt flow lobes (red, oranges, and yellow irregular bands on crater floor) on the floor of an impact crater containing a central pit at 28.5°N, 83.4°E. (For interpretation of the references to color in this figure legend, the reader is referred to the web version of this article.)

Greeley et al. (1982), and Schultz (1988) explosive models that would each emplace pit-derived ejecta around them, and the thermal inertia trend does not support the drainage and collapse models of Croft (1981) and Passey and Shoemaker (1982) that do not predict a distribution of pit-derived ejecta. However, each explosive model also suffers from a critical weakness. The Wood et al. (1978) model for an explosive pit origin suffers from the difficulty of keeping vapor from escaping early in the impact process before a pit can be preserved. The Greeley et al. (1982) central peak detachment model also suffers from issues scaling up from the laboratory to planetary impact craters. The Schultz (1988) low velocity impact model also suffers from scaling issues with respect to crater modification and material strength.

Alternatively, an explosive reaction could potentially result from mixing of water–ice and molten rock through several mechanisms. For example, a post-impact magmatic intrusion could intrude into a crater and react with the ground water as a maar volcano (Wohletz, 1986; Begét et al., 1996); however, we would not expect such a scenario to consistently form pits in crater centers. Heavy fracturing and brecciation during the impact process may allow fluids (either impact melt, or liquid water) to mobilize and permeate the substrate and come into contact with each other, similar to the fluid flow described by Elder et al. (2012). Although liquid water may move freely through fractures, Elder et al. finds that impact melt would cool too quickly due to its high melting temperature and larger temperature difference with the country rock. Rain or ice-bearing fallback ejecta could also be deposited on top of impact melt pools or suevite deposits (Segura et al., 2002), but that would not necessarily require that pits always form in the centers of their host craters, nor that they be consistently sized. Below, we describe an alternate model for bringing water into contact with impact melt.

## 6. Melt-contact model

We present an alternate hypothesis that – unique among other explosive pit origin hypotheses – predicts an explosion late enough in the impact process for central pits to be preserved and has a properly scaled analog. In our melt contact model, impact central uplifts bring water (as liquid, ice, or both) vertically up and into contact with near-surface impact melt to initiate late-stage steam explosions and form central pits (Fig. 10). Central uplift occurs late in the impact process from the end of the excavation stage through the modification stage, after most crater fill has settled (*e.g.*, Melosh, 1989); thus, pit formation concurrent with central uplift is consistent with the apparent lack of infilling of deep pits. As we describe in the next paragraph, our explosive central pit model is akin to an inverted maar volcano (*e.g.* White and Ross, 2011), except instead of magma rising up into contact with groundwater or permafrost, a water-bearing substrate is uplifted into contact with impact melt. Similarly-scaled events have been observed at monogenetic maar volcanoes with diameters of up to 8 km on the Seward Peninsula in Alaska (Begét et al., 1996), where the permafrost buffers the water-magma interaction to achieve high heat transfer efficiencies (Wohletz, 1986).

As the central uplift rises, it brings deeply-sourced water-bearing rock from below the transient cavity up into contact with shallow crater fill deposits and impact melts. We would not expect significant vertical mixing of sub-transient cavity material outside the central uplift, so these large pits should always be in the centers of their host impact craters. As the water-bearing central uplift rises into contact with impact melt and other hot debris, the thermal energy from the melt may be transferred to the water, resulting in a steam explosion to eject material outward, raise rims, and deposit ejecta surrounding the pits (with average grain sizes decreasing with radial distance, as we found in this study). As material is ejected outwards, the walls may become unstable and slump hot debris and impact melt into the pit cavity. There, the new rush of melt and hot rocks may again react with uplifting water to recharge the system and iteratively trigger a series of explosions to further deepen and widen the central pit. When central uplift slows, the vertical mixing of water decreases and the explosions will cease.

We explored the theoretical plausibility of whether enough thermal energy could have been available in a post-impact environment to initiate steam explosions capable of creating kilometer-scale central pits. We started with the empirical model shown below which predicts the mass ratio of melted ($m_m$) to displaced ($m_d$) impact target materials in a silicate target (Eq. (1)) (O'Keefe and Ahrens, 1982; Melosh, 1989):

$$m_m/m_d = 1.6 \times 10^{-7} \times (g \times D_i)^{0.83} \times v_i^{0.33}, \quad (1)$$

where $g$ is planetary gravity, $D_i$ is host crater diameter and $v_i$ is bolide velocity. We assigned the following values for our calculations: gravity $g = 3.711$ m/s$^2$ and mean Mars asteroidal bolide velocity $v_i = 10$ km/s (Ivanov et al., 2002). We also assumed that any melt generated remained within the host crater. Finally, we modeled the host crater as a half-ellipsoid and applied the mass fraction to determine the volume and mass of melt produced (Eqs. (2) and (3)):

$$V_m = (m_m/m_d) \times (2/3) \times \pi \times d_i \times (D_i/2)^2 \quad (2)$$

and

$$m_m = \rho_m/V_m, \quad (3)$$

where $V_m$ is the volume of melt, $d_i$ is the depth of the host crater, and $\rho_m$ is the density of the melt. We assumed a depth of complex craters (in km) of $d_i = 0.357 D_i^{0.52}$ (Tornabene et al., 2013). Sato and Taniguchi (1997) found the following empirical equation to predict the energy required to form a crater via volcanic, nuclear, and chemical explosions, independent of origin. The equation can similarly be applied to central pits (Eq. (4)):

$$E_c = 4.45 \times 10^6 \times D_p^{3.05}, \quad (4)$$

where $E_c$ is the energy of pit formation and $D_p$ is the diameter of the pit, for which we assume a median pit-to-host crater diameter ratio

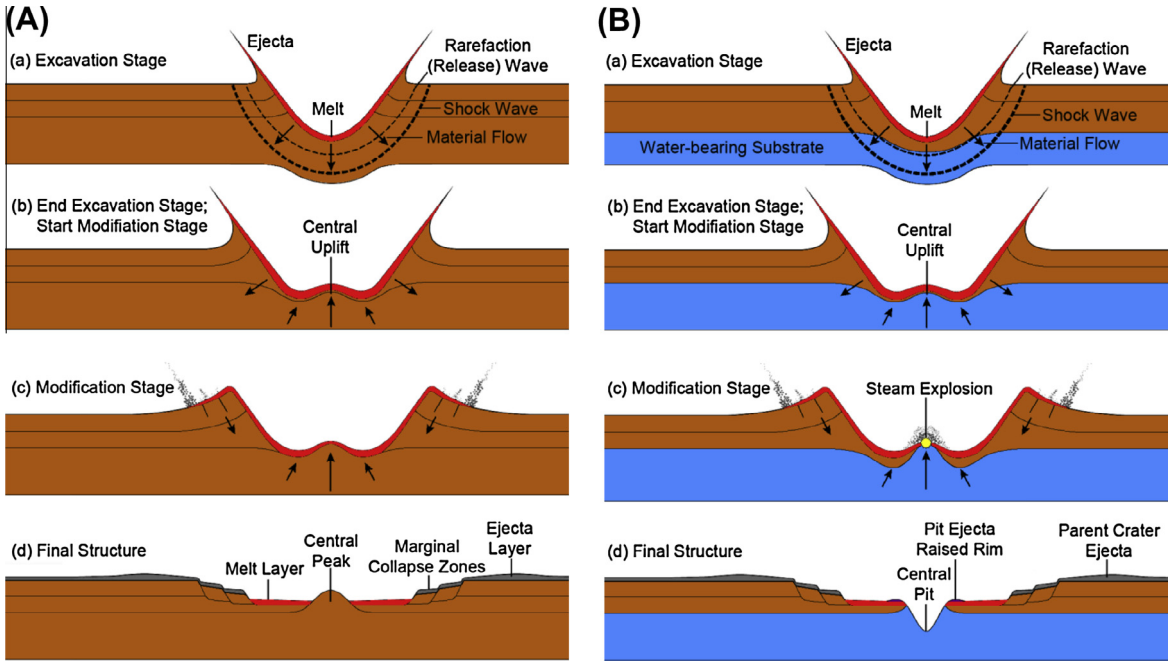


**Fig. 10.** Schematic cartoons illustrating steps in complex crater formation resulting in: (A) a classical central peak (modified from French, 1998) and (B) our proposed new "melt contact model" for martian central pit crater formation.

of 0.16 (Barlow, 2010, 2011). The total thermal energy transfer required to melt ice and boil water to steam can be calculated using specific and latent heats (*e.g.* Wohletz, 1986) (Eq. (5)):

$$H_w = m_w \times L_f + m_w \times c_{lq} \times \Delta T_w + m_w \times L_v, \quad (5)$$

where $H_w$ is the energy transferred to the water, $m_w$ is the mass of water, $L_f$ is the latent heat of fusion, $c_{lq}$ is the specific heat of liquid water, $\Delta T_w$ is the temperature change of liquid water, and $L_v$ is the latent heat of vaporization. We assigned values for $L_f = 3.34 \times 10^5$ J/kg, $c_{lq} = 4.187 \times 10^3$ J/kg K, and $L_v = 2.257 \times 10^6$ J/kg (Moran et al., 2010). We assumed thermal equilibrium between water and chilled impact melt, a saturated water (liquid–vapor) system, and a 100 K temperature change. Evaluating Eq. (5), we found that an investment of $3.023 \times 10^6$ J is required to turn 1 kg of water from ice (273 K) to steam (373 K). Steam could potentially be heated to higher temperatures and/or further pressurized, which would result a smaller amount of (superheated) steam to satisfy the energy requirements for explosivity. The thermal energy of vaporization, specifically the step of converting water to steam, can be transformed to kinetic energy that can form a pit. The mass of steam required is calculated by dividing the pit formation energy from Eq. (4) by the latent heat of vaporization. Dividing this result by the density of ice provides the volume of ice required to form a central pit. As shown in Fig. 11, assuming a half-ellipsoidal pit geometry with the pit depth (in km) $d_p = 0.276 D_p^{0.68}$ (Tornabene et al., 2013), only a small amount of water (comprising 2–6% of a central pit's volume) would need to be vaporized to form a central pit for the host crater diameters observed (5–125 km (Barlow, 2011)).

The amount of thermal energy available in impact melt may also be calculated using specific heats (Eq. (6)):

$$E_m = m_m \times c_{pm} \times \Delta T_m = \rho_m \times V_m \times c_{pm} \times \Delta T_m, \quad (6)$$

where $E_m$ is the energy required for cooling rock, $c_{pm}$ is the specific heat of rock, $\Delta T_m$ is the temperature change of the rock. We assumed a basaltic melt composition and assign values of $\rho_m = 2900$ kg/m$^3$ (Judd and Shakoor, 1989); $c_{pm} = 1000$ J/kg K (Wohletz, 1986); and change of temperature (from the basalt solidus to the STP boiling point of water) $\Delta T_m = 1473$ K − 373 K = 1100 K (Wohletz, 1986). It should be noted that impact melts can also be superheated, perhaps up to 1700 °C (1973 K) (Zieg and Marsh, 2005), so our calculations may underestimate the thermal energy available by ~50%. Adiabatic heat transfer efficiency is typically ~0.1 or less due to poor mixing; however, it can reach an optimal efficiency of ~0.3 for water/melt ratios of 0.3–0.5 (Wohletz, 1986). Such optimal efficiencies are believed to be present for maars in permafrost, as suggested by the largest, kilometer-scale terrestrial maars found in the Seward Peninsula, Alaska (Begét et al., 1996). Our calculations consider cases with both 0.1 (suboptimal) and 0.3 (optimal) efficiencies.

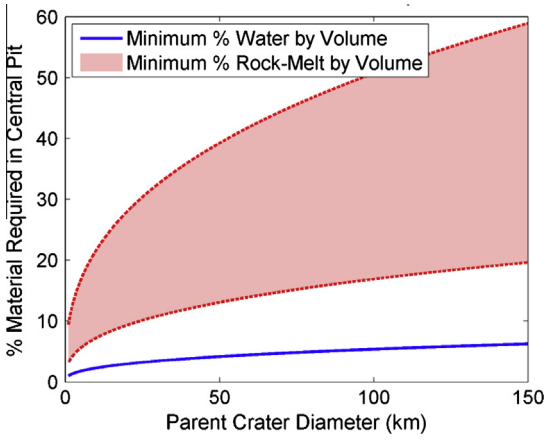


**Fig. 11.** Required amounts of water and impact melt for heat energy transfer to form a kilometer-scale (pit) crater shown as percent by volume with respect to the volume of a central pit crater. The range in impact melt volume represents uncertainty due to varying heat transfer efficiency between 0.1–0.3.

The mass of impact melt required to vaporize ice to steam can be calculated by setting the total heat transfer $H_w$ from Eq. (5) equal to the product of the heat transfer efficiency and the impact melt thermal energy from Eq. (6). As shown in Fig. 11, the impact melt must comprise a volume greater than or equal to 6–18% of the

central pit's volume for an optimal thermal efficiency of 0.3, or 17–55% of the central pit's volume for a suboptimal thermal efficiency of 0.1. The total energy transfer required for vaporizing ice ($H_w$) from Eq. (5) can also be compared to the total energy available from impact melt by multiplying Eq. (6) with the value(s) for heat transfer efficiency (Figs. 12 and 13). Based on these calculations, sufficient thermal energy should be available via impact melt to vaporize small amounts of ice that act explosively to form central pits within kilometer-scale impact structures. However, not all martian craters exhibit central pits. Below, we discuss the material requirements that may inhibit the explosive formation of some central pits on Mars.

First, an appropriate volume of water must be available in the central uplift. If too little water (or too low a concentration) is present, there may not be sufficient steam to form a large pit. Even if water was initially present in the target rocks, large impacts (with crater diameters of several tens to hundreds of km) likely remove most subsurface volatiles early in the impact process such that not enough water is available to react with the impact melt to form a pit. Conversely, if the system has excess water, there may not be enough thermal energy in the impact melt to heat the excess water and still vaporize enough to sustain an explosion and make a pit.

Second, an appropriate volume of impact melt must be retained within the host impact crater. Smaller impact craters produce less melt proportionally and distribute that impact melt more sparsely, so small craters may not have enough consolidated impact melt even if enough water is present. Larger impact craters might also produce excess impact melt that could fill in any central pits that might form. Another interesting aspect of the melt contact model is that since our calculations show it only requires small amounts of water (perhaps as little as 2–6% by volume), it provides a possible explanation for the formation of the small number of central pits observed on Mercury (Schultz, 1988; Xiao and Komatsu, 2013) and the Moon (Croft, 1981; Schultz, 1976a,b, 1988; Xiao et al., 2014), which should have insufficient water or other volatiles to form by drainage and collapse models (*e.g.* Croft, 1981). Although we did not measure summit pit-related thermal inertias in our survey, summit pits would be expected to form as in our melt contact model when steam explosions start but become water- or impact melt-limited. In such a case, the explosive reaction fails before uplift has ceased and an incomplete pit is left superposed on a remnant central peak.

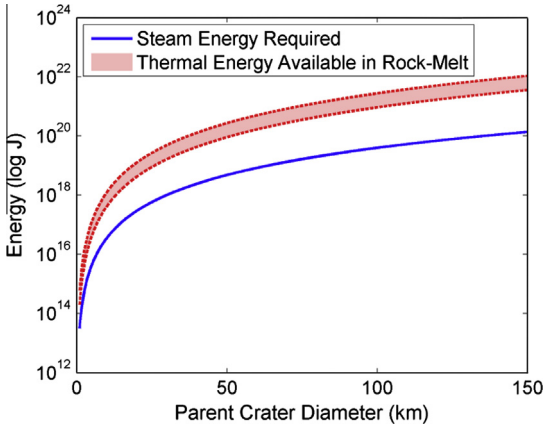


**Fig. 12.** Thermal energies of water required to convert ice to steam to provide the energy for creating central pit craters (blue line) of differing diameter. Also shown is the available thermal energy from impact melt, after applying thermal efficiency values of 0.1 (lower red curve) to 0.3 (upper red curve). (For interpretation of the references to color in this figure legend, the reader is referred to the web version of this article.)

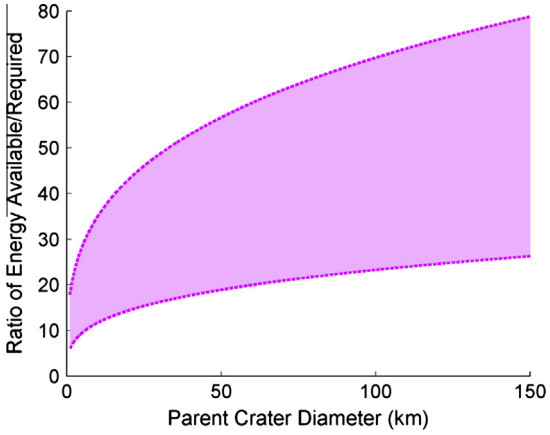


**Fig. 13.** Ratios of available/required thermal energy for vaporizing enough steam to explode and form a central pit, with respect to crater diameter. The range of in energy ratios reflects variations in heat transfer efficiency over a range of 0.1 (lower curve) to 0.3 (upper curve).

Based on our melt contact model, we propose the following testable predictions. First, the ejecta deposit is expected to contain abundant fractured and fragmented glassy impact melt, similar to the Onaping Formation at Sudbury (Grieve et al., 2010). This layer of glassy deposits should overlay more coherent impact melt deposits. Second, lithic clasts and mineral assemblages found stratigraphically below the transient crater should be found on the floor of the host crater, with the greatest abundance proximal to the rim. Third, the stratigraphic sequence of rocks around central pits should be overturned. Finally, *in situ* measurements of material around the pit should show decreasing average grain sizes with radial distance from central pits.

## 7. Conclusions

The presence of raised rims and blocky material surrounding martian central pits are suggestive of ejecta from an explosive pit origin. A strong majority of central pits in our global survey have material with radially decreasing thermal inertias around them, particularly for central pits craters with larger diameters and in regions relatively free of sand and dust. The population of central pit craters as a whole has a statistically significant ($P < 0.01$) decrease in thermal inertia radially outwards from pit rims. We interpret these findings as a typical decrease in average grain size with increasing distance away from central pits. As expected, dust masks the diurnal thermal signature around many central pits. This effect is amplified in smaller pits due to their less voluminous and finer-grained ejecta that are more easily buried or eroded.

Previously proposed models do not satisfactorily explain all observed characteristics of central pits. We have therefore proposed a new "melt contact model" to explain the observed morphologies (i.e., geometries, raised rims) and thermal properties (radially decreasing thermal inertias/average grain size) of martian central pit craters. Our thermal calculations show that only 2–6% water by volume is required to create a phreatomagmatic explosion and form central pits. The absence of central pits in many impact craters may be due to excess or insufficient volumes of impact melt and water to propagate a steam reaction, as well as variable degrees of mixing. Our explosive origin model is advantageous over drainage and collapse models in explaining the small number of central pits on Mercury and the Moon using only minor amounts of volatiles in localized pre-impact subsurfaces. Our melt contact model is also advantageous over other explosive models in forming the pit late enough in the impact process to be preserved.

Drainage and collapse may still be a viable method for pit formation on icy satellites, but an explosive origin appears to be the more viable mechanism on Mars (and other rocky planets) for forming central pit craters.

## Acknowledgments

We gratefully acknowledge Robin Fergason for her work on the THEMIS thermal inertia mosaic, JMARS development team, and the THEMIS, CTX, and HiRISE teams. We would also like to extend a special thank you to Devon Burr and Nadine Barlow for their invaluable time in reviewing and improving this manuscript.

## References

Alzate, N., Barlow, N.G., 2011. Central pit craters on Ganymede. Icarus 211, 1274–1283.
Baloga, S.M., Fagents, S.A., Mouginis-Mark, P.J., 2005. Emplacement of martian rampart crater deposits. J. Geophys. Res. 110, E10001. http://dx.doi.org/10.1029/2004JE002338.
Barlow, N.G., 2006. Impact craters in the northern hemisphere of Mars: Layered ejecta and central pit characteristics. Met. Planet. Sci. 41, 1425–1436.
Barlow, N.G., 2010. Central pit craters: Observations from Mars and Ganymede and implications for formation models. GSA Special Papers 465, 15–27.
Barlow, N.G., 2011. Constraints on the proposed formation models for martian central pit craters. Lunar Planet. Sci. 42. Abstract #1149.
Barlow, N.G., Bradley, T.L., 1990. Martian impact craters: Correlations of ejecta and interior morphologies with diameter, latitude, and terrain. Icarus 87 (1), 156–179.
Barlow, N.G. et al., 2000. Standardizing the nomenclature of martian impact crater ejecta morphologies. J. Geophys. Res. 105 (E11), 26733–26738.
Begét, J.E., Hopkins, D.M., Charron, S.D., 1996. The largest known maars on Earth, Seward Peninsula, northwest Alaska. Arctic 49 (1), 62–69.
Bell III, J.F. et al., 2013. Calibration and performance of the Mars Reconnaissance Orbiter Context Camera (CTX). Mars 8, 1–14. http://dx.doi.org/10.1555/mars.2013.0001.
Boyce, J.M., Wilson, L., Mouginis-Mark, P.J., Hamilton, C.W., Tornabene, L.L., 2012. Origin of small pits in martian impact craters. Icarus 221 (1), 262–275.
Boynton, W.V. et al., 2007. Concentration of H, Si, Cl, K, Fe, and Th in the low- and mid-latitude regions of Mars. J. Geophys. Res. 112, E12S99. http://dx.doi.org/10.1029/2007JE002887.
Bray, V.J., 2009. Impact Crater Formation on the Icy Galilean Satellites. Doctoral Dissertation, Imperial College London.
Bray, V.J., Schenk, P.M., Melosh, H.J., Morgan, J.V., Collins, G.S., 2012. Ganymede crater dimensions – Implications for central peak and central pit formation and development. Icarus 217, 115–129.
Buhl, E., Sommer, F., Poelchau, M.H., Dresen, G., Kenkmann, T., 2014. Ejecta from experimental impact craters: Particle size distribution and fragmentation energy. Icarus 237, 131–142.
Carr, M.H., Crumpler, L.S., Cutts, J.A., Greeley, R., Guest, J.E., Masursky, H., 1977. Martian impact craters and emplacement of ejecta by surface flow. J. Geophys. Res. 82 (28), 4055–4065.
Caudill, C.M., Tornabene, L.L., McEwen, A.S., Byrne, S., Ojha, L., Mattson, S., 2012. Layered MegaBlocks in the central uplifts of impact craters. Icarus 221 (2), 710–720.
Christensen, P.R., 1986. The spatial distribution of rocks on Mars. Icarus 68, 217–238.
Christensen, P.R. et al., 2001. Mars global surveyor Thermal Emission Spectrometer experiment: Investigation description and surface science results. J. Geophys. Res. 106 (E10), 23823–23871.
Christensen, P.R. et al., 2004. The Thermal Emission Imaging System (THEMIS) for the Mars 2001 Odyssey mission. Space Sci. Rev. 110, 85–130.
Christensen, P.R., et al., 2009. JMARS – A planetary GIS. American Geophysical Union (Fall). Abstract # #IN22A-06.
Clifford, S.M., Hillel, D., 1983. The stability of ground ice in the equatorial region of Mars. J. Geophys. Res. 88 (B3), 2456–2474.
Croft, S.K., 1981. On the origin of pit craters. Proc. Lunar Sci. Conf. 12, 196–198.
Cushing, G.E., Titus, T.N., Wynne, J.J., Christensen, P.R., 2007. THEMIS observes possible cave skylights on Mars. Geophys. Res. Lett. 34, L17201. http://dx.doi.org/10.1029/2007GL030709.
Edwards, C.S., Bandfield, J.L., Christensen, P.R., Fergason, R.L., 2009. Global distribution of bedrock exposures on Mars using THEMIS high-resolution thermal inertia. J. Geophys. Res. 114, E11001. http://dx.doi.org/10.1029/2009JE003363.
Edwards, C.S., Nowicki, K.J., Christensen, P.R., Hill, J., Gorelick, N., Murray, K., 2011. Mosaicking of global planetary image datasets: 1. Techniques and data processing for Thermal Emission Imaging System (THEMIS) multi-spectral data. J. Geophys. Res. 116, E10008. http://dx.doi.org/10.1029/2010JE003755.
Elder, C.M., Bray, V.J., Melosh, H.J., 2012. Theoretical plausibility of central pit crater formation via melt drainage. Icarus 221, 831–843.
Fergason, R.L., Christensen, P.R., Kieffer, H.H., 2006. High resolution thermal inertia derived from THEMIS: Thermal model and applications. J. Geophys. Res. 111, E12004. http://dx.doi.org/10.1029/2006JE002735.
French, B.M., 1998. Traces of Catastrophe. LPI Contribution No. 954, Lunar Planet. Inst., Houston, Texas.
Garner, K.M.L., Barlow, N.G., 2012. Distribution of rimmed, partially rimmed, and non-rimmed central floor pits on Mars. Lunar Planet. Sci. 43. Abstract #1256.
Garvin, J.B., Sakimoto, S.E., Frawley, J.J., 2000a. Craters on Mars: Global geometric properties from gridded MOLA topography. Mars 5. Abstract #3277.
Garvin, J.B., Sakimoto, S.E., Frawley, J.J., Schnetzler, C., 2000b. North polar region craterforms on Mars: Geometric characteristics from the Mars Orbiter Laser Altimeter. Icarus 144 (2), 329–352.
Gault, D.E., Greeley, R., 1978. Exploratory experiments of impact craters formed in viscous-liquid targets: Analogs for martian rampart craters? Icarus 34, 486–495.
Gault, D.E., Shoemaker, E.M., Moore, H.J., 1963. Spray Ejected from the Lunar Surface by Meteoroid Impact. NASA Technical Note D-1767.
Greeley, R., Fink, J.H., Gault, D.E., Guest, J.E., 1982. Experimental simulation of impact cratering on icy satellites. In: Morrison, D. (Ed.), Satellites of Jupiter. University of Arizona Press, Tucson, Arizona, pp. 340–378.
Grieve, R.A.F., Ames, D.E., Morgan, J.V., Artemieva, N., 2010. The evolution of the Onaping Formation at the Sudbury impact structure. Met. Planet. Sci. 45 (5), 759–782.
Head, J.W., Mustard, J.F., Kreslavsky, M.A., Milliken, R.E., Marchant, D.R., 2003. Recent ice ages on Mars. Nature 426, 797–802.
Hodges, C.A., 1978. Central pit craters on Mars. Proc. Lunar Sci. Conf. 9, 521–522.
Hodges, C.A., Shew, N.B., Clow, G., 1980. Distribution of central pit craters on Mars. Proc. Lunar Sci. Conf. 11, 450–452.
Ivanov, B.A., Neukum, G., Bottke, W.F., Hartmann, W.K., 2002. The comparison of size–frequency distributions of impact craters and asteroids and the planetary cratering rate. Asteroids III 1, 89–101.
Judd, W.R., Shakoor, A., 1989. In: Ho, C.Y. et al. (Eds.), Density in Physical Properties of Rocks and Minerals. Taylor and Francis, Philadelphia, PA, pp. 409–502.
Malin, M.C. et al., 2007. Context Camera investigation on board the Mars Reconnaissance Orbiter. J. Geophys. Res. 112, E05S04. http://dx.doi.org/10.1029/2006JE002808.
McEwen, A.S., Preblich, B.S., Turtle, E.P., Artemieva, N.A., Golombek, M.P., Hurst, M., Kirk, R.L., Burr, D.M., Christensen, P.R., 2005. The rayed crater Zunil and interpretations of small impact craters on Mars. Icarus 176, 351–381.
McEwen, A.S. et al., 2007. Mars Reconnaissance Orbiter's High Resolution Imaging Science Experiment (HiRISE). J. Geophys. Res. 112, E05S02. http://dx.doi.org/10.1029/2005JE002605.
Mellon, M.T., Jakosky, B.M., Postawko, S.E., 1997. The persistence of equatorial ground ice on Mars. J. Geophys. Res. 102 (E8), 19357–19369.
Melosh, H.J., 1989. Impact cratering: A geologic process. Oxford Monographs on Geology and Geophysics #11. Oxford University Press, New York.
Moran, M.J., Shapiro, H.N., Boettner, D.D., Bailey, M., 2010. Fundamentals of Engineering Thermodynamics. John Wiley & Sons.
O'Keefe, J.D., Ahrens, T.J., 1982. Cometary and meteorite swarm impact on planetary surfaces. J. Geophys. Res. 87 (B8), 6668–6680.
O'Keefe, J.D., Ahrens, T.J., 1985. Impact and explosion crater ejecta, fragment size, and velocity. Icarus 62, 328–338.
Okubo, C.H., Martel, S.J., 1998. Pit crater formation on Kilauea volcano, Hawaii. J. Volcanol. Geotherm. Res. 86, 1–18.
Passey, Q.R., Shoemaker, E.M., 1982. Craters and basins on Ganymede and Callisto: Morphological indicators of crustal evolution. In: Morrison, D. (Ed.), Satellites of Jupiter. Univ. of Arizona Press, Tucson, Arizona, pp. 379–434.
Pierazzo, E., Artemieva, N.A., Ivanov, B.A., 2005. Starting conditions for hydrothermal systems underneath martian craters: Hydrocode modeling. In: Kenkmann, T., Hörz, F., Deutsch, A. (Eds.), Large Meteorite Impacts III. Geo. Soc. of America, Boulder, CO, pp. 443–457.
Robinson, M.S. et al., 2012. Confirmation of sublunarean voids and thin layering in mare deposits. Planet. Space Sci. 69, 18–27.
Salvati, R., Sasowsky, I.D., 2002. Development of collapse sinkholes in areas of groundwater discharge. J. Hydrol. 264, 1–11.
Sato, H., Taniguchi, H., 1997. Relationship between crater size and eject volume of recent magmatic and phreato-magmatic eruptions: Implications for energy partitioning. Geophys. Res. Lett. 24 (3), 205–208.
Schultz, P.H., 1976a. Floor-fractured lunar craters. Moon 15, 241–273.
Schultz, P.H., 1976b. Moon Morphology. University of Texas Press, Austin, Texas.
Schultz, P.H., 1988. Cratering on mercury: A relook. In: Villas, F., Chapman, C.R., Matthews, M.S. (Eds.), Mercury. University of Arizona Press, Tucson, Arizona, pp. 274–335.
Segura, T.L., Toon, O.B., Colaprete, A., Zahnle, K., 2002. Environmental effects of large impacts on Mars. Science 298 (5600), 1977–1980.
Senft, L.E., Stewart, S.T., 2011. Modeling the morphological diversity of impact craters on icy satellites. Icarus 214, 67–81.
Sharpton, V.L., 2014. Outcrops on lunar crater rims: Implications for rim construction mechanisms, ejecta volumes and excavation depths. J. Geophys. Res. Planets 119, 154–168.
Smith, E.I., 1976. Comparison of the crater morphology–size relationship for Mars, Moon, and Mercury. Icarus 28, 543–550.
Smith, B.A. et al., 1979. The Galilean satellites and Jupiter: Voyager 2 imaging science results. Science 206, 927–950.
Smith, D.E. et al., 2001. Mars Orbiter Laser Altimeter: Experiment summary after the first year of global mapping of Mars. J. Geophys. Res. 106 (E10), 23689–23722.

Tornabene, L.L. et al., 2006. Identification of large (2–10) km rayed craters on Mars in THEMIS thermal infrared images: Implications for possible martian meteorite source regions. J. Geophys. Res. 111, E10006. http://dx.doi.org/10.1029/2005JE002600.

Tornabene, L.L., Osinski, G.R., McEwen, A.S., Boyce, J.M., Bray, V.J., Caudill, C.M., Grant, J.A., Hamilton, C.W., Mattson, S., Mouginis-Mark, P.J., 2012. Widespread crater-related pitted materials on Mars: Further evidence for the role of target volatiles during the impact process. Icarus 220 (2), 348–368.

Tornabene, L.L., Ling, V., Osinski, G.R., Boyce, J.M., Harrison, T.N., McEwen, A.S., 2013. A revised global depth-diameter scaling relationship for Mars based on pitted impact melt-bearing craters. Lunar Planet. Sci. 44. Abstract #2592.

White, J.D.L., Ross, P.-S., 2011. Maar-diatreme volcanoes: A review. J. Volcanol. Geotherm. Res. 201, 1–29.

Wohletz, K.H., 1986. Explosive magma–water interactions: Thermodynamics, explosion mechanics, and field studies. Bull. Volcanol. 48, 245–264.

Wohletz, K.H., Sheridan, M.F., 1983. Martian rampart crater ejecta: Experiments and analysis of melt–water interaction. Icarus 56, 15–37.

Wood, C.A., Head, J.W., Cintala, M.J., 1978. Interior morphology of fresh martian craters: The effects of target characteristics. Proc. Lunar Sci. Conf. 9, 3691–3709.

Xiao, Z., Komatsu, G., 2013. Impact craters with ejecta flows and central pits on Mercury. Plan. Space Sci. http://dx.doi.org/10.1016/j.pss.2013.03.015.

Xiao, Z., Zeng, Z., Komatsu, G., 2014. A global inventory of central pit craters on the Moon: Distribution, morphology, and geometry. Icarus 227, 195–201.

Zieg, M.J., Marsh, B.D., 2005. The Sudbury Igneous Complex: Viscous emulsion differentiation of a superheated impact melt sheet. Geol. Soc. Am. Bull. 117 (11–12), 1427–1450.